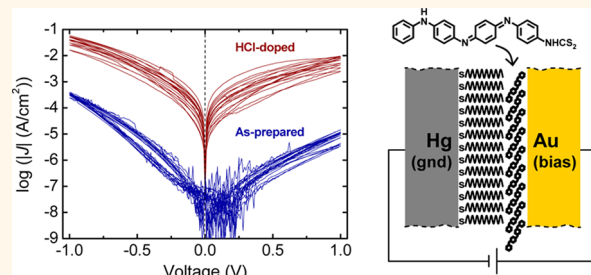


# Conductance Modulation in Tetraaniline Monolayers by HCl-Doping and by Field-Enhanced Dissociation of H<sub>2</sub>O

William E. Ford,\* Deqing Gao, Frank Scholz, Gabriele Nelles, and Florian von Wrochem\*

Materials Science Laboratory, Sony Deutschland GmbH, Hedelfinger Strasse 61, 70327 Stuttgart, Germany

**ABSTRACT** Oligoanilines are interesting candidates for organic electronics, as their conductivity can be varied by several orders of magnitude upon protonic doping. Here we demonstrate that tetraaniline self-assembled monolayers exhibit an unprecedented conductance on/off ratio of  $\sim 710$  (at  $+1$  V) upon doping of the layers from the emeraldine base to the emeraldine salt form. Furthermore, a pronounced asymmetry in the current–voltage characteristics indicates dynamic doping of the tetraaniline layer by protons generated through field-enhanced dissociation of water molecules, a phenomenon known as the second Wien effect. These results point toward oligoanilines as promising substitutes for polyaniline layers in next-generation thin film devices.



**KEYWORDS:** oligoaniline · molecular switch · self-assembled monolayer · protonic doping · dynamic doping · Wien effect · dithiocarbamate · Hg-drop technique

The pronounced dependence of the electrical conductivity of  $\pi$ -conjugated polymers on doping level and the ability to control this level is the basis for their application in a wide range of electronic and optical materials, exploitable in electrodes,<sup>1,2</sup> transistors,<sup>3,4</sup> memories,<sup>5,6</sup> and sensors.<sup>7,8</sup> Polyaniline (PANI) is unique among the common conjugated polymers because it can be switched between conductive ("on") and insulating or semiconductive ("off") states by protonation–deprotonation as well as by oxidation–reduction.<sup>9</sup> Modulation of the conductivity of PANI films *via* oxidation–reduction (electrochemistry) is the basis for devices with diode or transistor properties,<sup>10</sup> as well as memristive behavior,<sup>11</sup> while modulation *via* protonation–deprotonation provides sensing capabilities.<sup>7</sup>

As miniaturization in organic semiconductor devices progresses, film thickness and homogeneity become critical factors in view of speed and reliability. In this respect, PANI suffers from poor solubility and polydispersity, making it difficult to prepare thin films with uniform thickness and electrical characteristics by using conventional methods such as drop- or spin-casting, *in situ* chemical deposition, or electrochemical

deposition,<sup>12,13</sup> Although thin films of PANI can be obtained using pulsed laser,<sup>14</sup> thermal evaporation,<sup>15</sup> or sputter deposition,<sup>16</sup> these processes result in the degradation of the polymer.<sup>14–16</sup> As a result, attention has turned to aniline oligomers (oligoanilines), which have electronic and optical properties similar to those of PANI<sup>17–19</sup> with the advantage of being monodisperse, soluble, readily functionalized, and crystallizable.<sup>20–26</sup> Compared to the parent polymer, however, little is known about the transport properties of oligoanilines, especially in thin films.

Here we investigate the conductivity of ultrathin monolayers, assembled from the emeraldine ("half-oxidized") aniline tetramer (tetraaniline, TANI) in its undoped (emeraldine base, EB) and doped (emeraldine salt, ES) form. In Hg-drop measurements, the TANI monolayers show an outstandingly high on/off conductance ratio ( $R_{\text{on/off}}$ ) when converted from the EB to the ES state. Furthermore, a significant rectification in their current–voltage characteristics is seen. This behavior is interpreted in light of a new type of dynamic doping caused by field-induced dissociation of water molecules located within the junction (the second Wien effect).<sup>27</sup> It is further demonstrated that dithiocarbamate (DTC) chemistry

\* Address correspondence to  
William.Ford@eu.sony.com,  
Florian.vonWrochem@eu.sony.com.

Received for review July 6, 2012  
and accepted February 19, 2013.

Published online February 19, 2013  
10.1021/nn3050769

© 2013 American Chemical Society

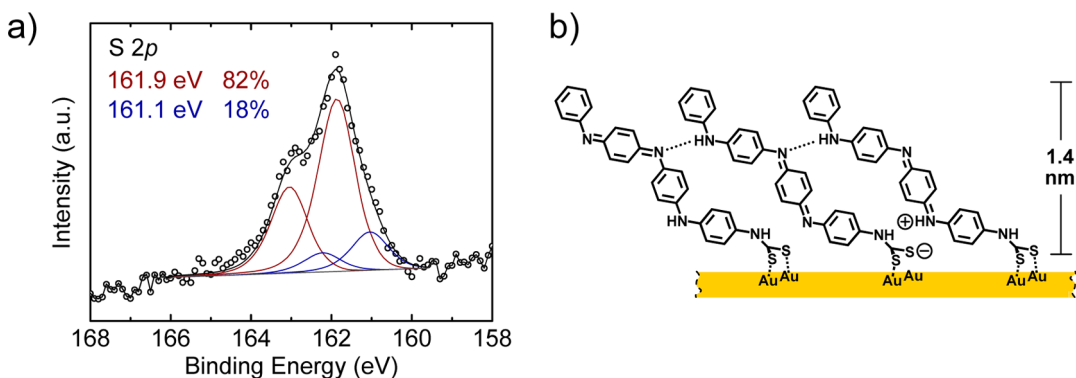


Figure 1. (a) XP-spectrum of the TANI-DTC monolayer in the S 2p core level region. (b) Structural model of the monolayer based on XPS data. It includes possible structural variations, such as isomeric/tautomeric combinations, intermolecular hydrogen bonding, and monodentate binding of the dithiocarbamate group to Au.

can be used to form TANI monolayers on gold substrates by simple self-assembly from solution, yielding monolayers that are chemically stable in both the EB and ES states.

## RESULTS AND DISCUSSION

Monolayers (SAMs) were formed by soaking freshly cleaved template-stripped gold substrates (RMS roughness of 0.3 nm)<sup>28</sup> in  $\sim 5 \times 10^{-4}$  M ethanolic solutions of TANI-DTC, which were prepared *in situ*<sup>29</sup> by adding nearly equivalent (2–3% excess) amounts of triethylamine and CS<sub>2</sub> to solutions of TANI. The as-prepared SAMs, which were in their undoped EB state (*vide infra*), were doped with HCl vapor by placing them in a covered vessel with a drop of concentrated hydrochloric acid for 1–3 min. The quality of the SAMs before and after doping was verified by X-ray photoemission spectroscopy (XPS). Several key findings of the XPS analysis are summarized here and further details can be found in the Supporting Information (section SI-1). The S 2p signal (Figure 1a) has a main component at a binding energy of 161.9 eV, demonstrating a bidentate coordination of both sulfur atoms of the dithiocarbamate group to Au.<sup>30</sup> The composition, corrected for photoelectron attenuation, is in excellent agreement with the predicted stoichiometry for TANI-DTC. The thickness (*d*) is estimated to be 1.4 nm by comparison of the attenuation of the Au 4f signal with that of a reference monolayer (see Table 1). In agreement with XPS data, Figure 1b shows the proposed structural model of the SAM, with TANI having an average molecular tilt angle of  $\sim 50^\circ$  with respect to the surface normal. It is important to note that the XP spectrum of the HCl-doped SAM was essentially identical to that of the undoped SAM described above. This observation leads to two conclusions: (1) HCl dissociates from the monolayer when kept in ultrahigh vacuum for several hours, and (2) the dithiocarbamate group is chemically stable in both the undoped and doped states of the SAM. Additional topographic and spectroscopic characterization of the monolayers was carried out by STM, PM-IRRAS, and ellipsometry (Supporting Information, section SI-1).

Current density–voltage (*J*–*V*) characteristics were obtained using Hg-drop top electrodes, as shown schematically in Figure 2a.<sup>30,31</sup> Before making contact, the Hg-drop was suspended in a solution of hexadecanethiol (HSC<sub>16</sub>H<sub>33</sub>) to coat the mercury surface with a thiolate monolayer, which serves as a spacer between Hg-drop and TANI-DTC layer and thus reduces the probability for electrical shorts. The reproducibility of the electrical data before and after doping indicates that the monolayers are free of defects that could cause shorts. It also indicates that the SAMs are not prone to decomposition by protonation (also verified by XPS, as noted above). Log |*J*|–*V* plots obtained before and after doping with HCl vapor are shown in Figure 2b. The values of *R*<sub>on/off</sub> at +1 V is  $710 \pm 120$ , based on averages of data sets for doped and undoped TANI-DTC layers (see Supporting Information, Figure S6). The results from electrical measurements are summarized in Table 1 together with data acquired with junctions including two reference monolayers (*vide infra*).

The *J*–*V* characteristics exhibit hysteresis in both the doped and undoped (as-prepared) states, for positive and negative voltages. Since other junctions, including known reference SAMs instead of TANI-DTC (e.g., alkanethiols, aromatic dithiocarbamates), do not show any hysteresis (see Supporting Information, Figures S10 and S11) this behavior is attributed to the TANI-DTC monolayer. The hysteresis can be interpreted in terms of a dynamic doping model (*vide infra*), being the result of thermodynamic trapping of H<sup>+</sup> and OH<sup>–</sup> ions within the TANI-DTC layer (see Supporting Information, section SI-8).

Another prominent feature of the *J*–*V* data is the decrease of the current density (*J*) with time (*t*) after immersion of the TANI-DTC SAMs in the bath solution that is used during Hg-drop measurements. Figure 3 shows two examples of the dependence of *J* on *t*. To probe the short immersion-time regime, the hexadecanethiol SAM was preformed on an Hg electrode (for  $\sim 10$  min) and the sample was immersed into the solution shortly before measurement (curve a). When

**TABLE 1. Electrical Properties of Undoped and HCl-doped TANI-DTC SAMs and of Two Reference Monolayers<sup>a</sup>**

SAM	SAM thickness <sup>b</sup> (nm)	junction configuration for $J$ – $V$ measurements <sup>c</sup>	$J_{\text{off}}$ (A/cm <sup>2</sup> )	$J_{\text{on}}$ (A/cm <sup>2</sup> )	$R_{\text{on/off}}$
TANI-DTC	1.4 ± 0.1	Hg SC <sub>16</sub> H <sub>33</sub>   TANI-DTC Au	$4.3_2 \times 10^{-7}$ <sup>d</sup> $9.0_6 \times 10^{-6}$ <sup>e</sup>	$8.5_4 \times 10^{-4}$ <sup>d</sup> $6.4_8 \times 10^{-3}$ <sup>e</sup>	1980 <sup>d</sup> 710 <sup>e</sup>
C <sub>12</sub> H <sub>25</sub> SH <sup>f</sup>	1.4 ± 0.1	Hg SC <sub>16</sub> H <sub>33</sub>   C <sub>12</sub> H <sub>25</sub> S Au		$3.3_2 \times 10^{-7}$ <sup>d</sup>	
TPM-DTC <sup>g</sup>	1.7 ± 0.1	Hg SC <sub>16</sub> H <sub>33</sub>   TPM-DTC Au		$1.1_2 \times 10^{-3}$ <sup>d</sup>	

<sup>a</sup> Bias voltages were applied to the Au bottom electrode, with the Hg-drop serving as ground. All  $J$  values listed here were measured at positive bias. <sup>b</sup> The film thickness of the TANI-DTC monolayer was determined by XPS. <sup>c</sup> Configuration of the junction during Hg-drop measurements, where “||” represents an interface with a covalent metal–organic bond and “||” represents an interface between two layers in van der Waals contact. <sup>d</sup> Values evaluated at  $V = +0.5$  V during the down-sweep.  $J_{\text{off}}$  refers to as-prepared samples and  $J_{\text{on}}$  refers to HCl-doped samples; these distinctions do not apply to the two reference systems. <sup>e</sup> Values evaluated at  $V = +1$  V. <sup>f</sup> The thickness of the dodecanethiol SAM was estimated as the molecular length multiplied by  $\cos(30^\circ)$ . <sup>g</sup> Data for *N*-methyl-[1,1':4',1'']terphenyl-4''-methyl)dithiocarbamate (TPM-DTC) are from ref 30.

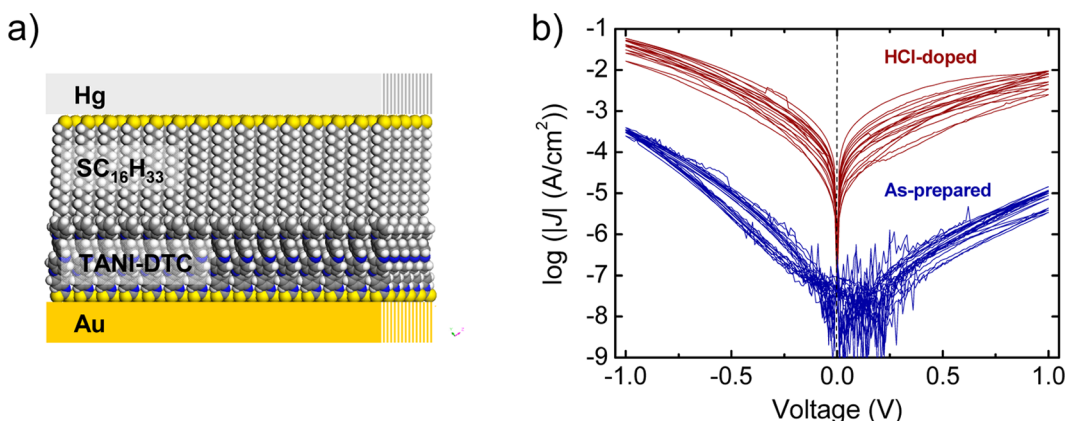


**Figure 2.** (a) Model of the TANI-DTC molecular junction during electrical characterization with the Hg-drop setup. (b) Semilog plot of the absolute current density versus bias voltage for HCl-doped and for as-prepared (undoped) TANI-DTC monolayers. Each individual curve represents data obtained from a different sample. The HCl-doped samples were, on average, exposed to the solution for 25–30 min before the  $J$ – $V$  characteristics were measured.

sample and Hg electrode were immersed into solution at the same time, longer exposure times were required (curve b). The values of  $J$  (at either  $-1$  or  $-0.5$  V) were obtained during successive  $J$ – $V$  sweeps, while maintaining contact between the two electrodes. Curves a and b in Figure 3 are first-order exponential decay fits to the  $J$ – $t$  data, resulting in  $k = 0.21$  min<sup>-1</sup> and  $k = 0.13$  min<sup>-1</sup>, respectively. We attribute the decay in conductivity to the loss of HCl from the TANI-DTC SAM. However, the fits converge to values of  $J$  that are significantly higher than those observed for undoped TANI-DTC SAMs (*i.e.*, by a factor of  $\sim 10^2$ ), meaning that the final state still corresponds to partially doped TANI. The dedoping of the SAM appears to require the liquid bath environment, since the doped TANI-DTC film is stable in dry air for several hours, as observed by infrared spectroscopy (Supporting Information, section SI-1). Both fit curves in Figure 3 indicate that the initial  $J$  (at  $t = 0$  min) is about 2.8 times higher than  $J$  after exposure to solution for 10 min. Since in our  $J$ – $V$  data (Figure 2b) the first scan was typically acquired after a delay time of  $\sim 10$  min, the extrapolated value of  $R_{\text{on/off}}$  for the initial doping level is estimated to be  $\sim 2.8$  times higher than the experimentally determined value; that is,  $R_{\text{on/off}} \approx 2.8 \times 710 = 2000$  (at  $V = +1$  V). Even though this ratio is small compared to the value of

$10^6$ – $10^7$  observed for thin PANI films,<sup>14</sup> it is significantly higher than the values reported for oligoaniline strands that are switched electrochemically ( $R_{\text{on/off}} \approx 70$ – $100$ )<sup>32</sup> or PANI nanofibers that are doped with HCl ( $R_{\text{on/off}} \approx 80$ ).<sup>33</sup> Using TANI-DTC SAMs in a solid-state, sealed device structure would probably allow the long-term stability in either doping state, as indicated by the above-mentioned IR data.

The reason for the lower  $R_{\text{on/off}}$  in TANI-DTC monolayers compared to bulk PANI, where  $R_{\text{on/off}}$  can reach values of  $10^9$ – $10^{10}$ , is of great interest for a fundamental understanding of charge transfer processes occurring in this type of material at different length scales. To address this issue, the above  $J$ – $V$  characteristics are related to those from junctions using monolayers of either *N*-methyl-[1,1':4',1'']terphenyl-4''-ylmethyl)dithiocarbamate (TPM-DTC) ( $d \approx 1.7$  nm)<sup>30</sup> or dodecanethiol ( $d \approx 1.4$  nm) in place of TANI-DTC (Table 1 and Supporting Information Figures S10 and S11). On the basis of this comparison, we find that the as-prepared TANI-DTC SAM is  $\sim 1.3$  times more conductive than a SAM of 1-dodecanethiol (based on  $J$  at  $+0.5$  V), which is consistent with the insulating nature of the EB state of PANI<sup>9</sup> and shows that the TANI monolayer is in the expected EB state. On the other hand, the measured conductivity of a HCl-doped TANI-DTC SAM is  $\sim 0.8$  times that of a monolayer of TPM-DTC,

one of the most conductive aromatic compounds.<sup>30</sup> Theoretical<sup>34</sup> and experimental<sup>19,35</sup> investigations indicate that for TANI the highest occupied molecular orbital of the

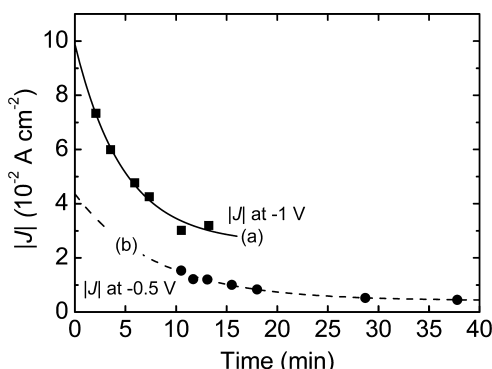


**Figure 3.** Dependence of  $|J|$  of HCl-doped TANI-DTC SAMs on time during Hg-drop measurements. (a)  $J$  measured at  $-1\text{ V}$  after the immersion (at  $t = 0$ ) of the SAM into the solution. The first scan was acquired at  $\sim 2$  min after immersion. The line is a least-squares fit following the first-order exponential decay  $J(t) = 0.0254 + 0.0736 \exp(-t/4.82)$ . (b)  $J$  measured at  $-0.5\text{ V}$  after the immersion (at  $t = 0$ ) of the SAM into the solution. The first scan was acquired at  $\sim 10$  min after immersion. The line is a least-squares fit following the first-order exponential decay  $J(t) = 0.00419 + 0.0394 \exp(-t/7.96)$ .

ES state is delocalized as a bipolaron that spans the four N-atoms (all of which are protonated) and the three inner phenyl rings, causing the observed high conductivity. In contrast, charge transport through a TPM-DTC layer is known to occur by nonresonant tunneling across the  $\pi$ -system.<sup>30,36</sup> Despite that a quantitative understanding of charge transport in ultrathin oligoaniline layers is not yet established, our findings indicate that bipolaronic transport controls the electrical behavior of oligoaniline assemblies, even down to the molecular length scale ( $\sim 2\text{ nm}$ ) that is characteristic of two-terminal, monolayer junctions.

The ability of PANI films to have their electrical conductivity switched repeatedly between “on” and “off” states by exposure to acids and bases is the basis for the interest in using the films as active elements of environmental sensors.<sup>7,8</sup> To test whether the TANI-DTC monolayers could also be switched, we examined their  $J$ - $V$  characteristics upon sequential exposure to HCl and  $\text{NH}_3$  vapors. An example of one of these experiments is provided in the Supporting Information (section SI-3). Although switching was demonstrated, after the second doping step degradation is observed in the  $J$ - $V$  characteristics. We believe, however, that the degradation is primarily due to the rinsing procedure used to remove the hexadecane

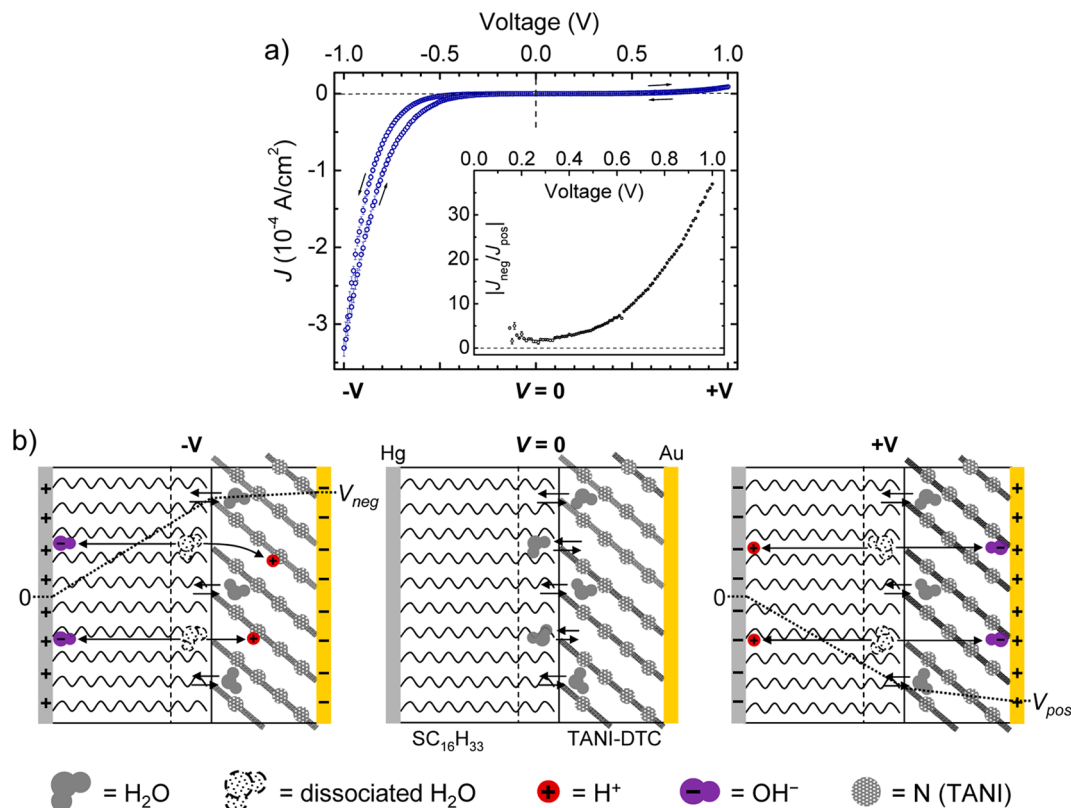


**Figure 4.** (a)  $J$ - $V$  curve for the as-prepared (EB-form) TANI-DTC SAM. The data is the average of the curves presented in Figure 2b. The inset shows the ratio of  $|J|$  obtained at negative ( $J_{\text{neg}}$ ) and positive ( $J_{\text{pos}}$ ) bias as a function of the absolute bias  $|V|$ . (b) Schematic representations of the junction under negative, zero, and positive biases, illustrating the proposed dynamic doping model. Indicated are the dynamic distribution of  $\text{H}_2\text{O}$  molecules between the two SAMs, as well as the dissociation of  $\text{H}_2\text{O}$  molecules in the high  $E$ -field region and concomitant field-driven diffusion of the resulting  $\text{H}^+$  and  $\text{OH}^-$  ions. The dotted line indicates the voltage profile across the junction.

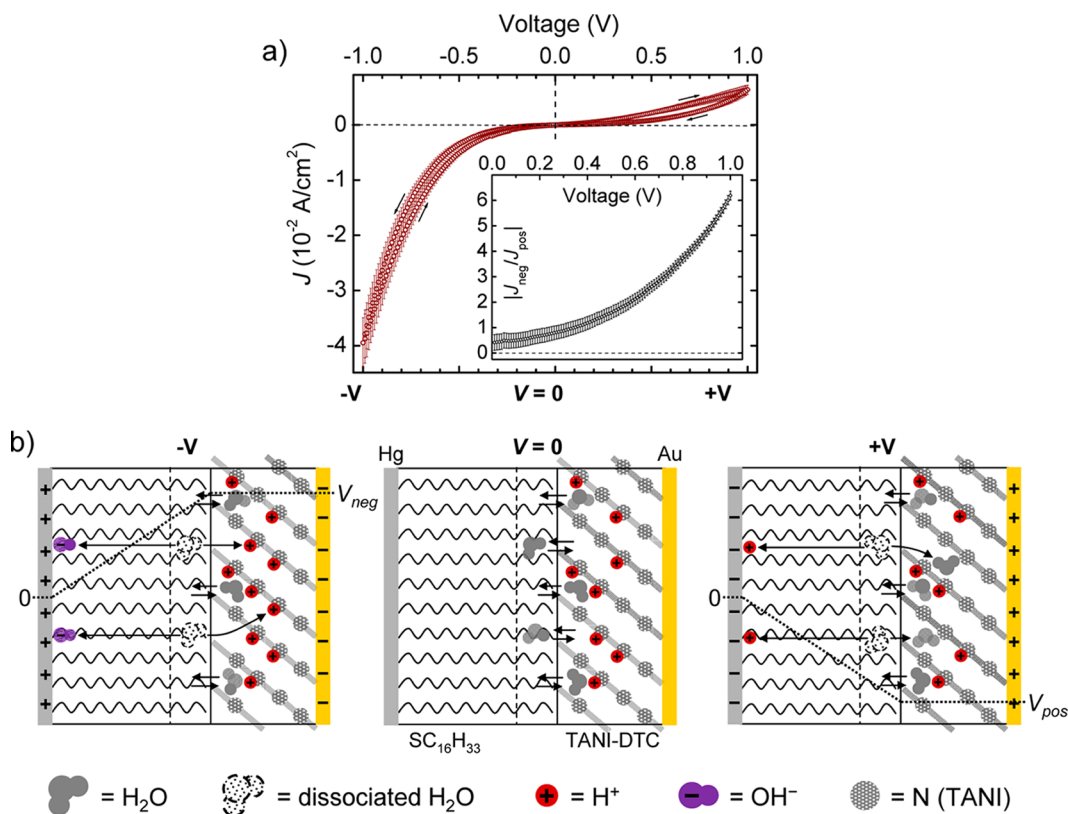


Figure 5. (a)  $J$ – $V$  curve for the HCl-doped (ES-form) TANI–DTC SAM. The data is the average of the curves presented in Figure 2b. The inset shows the ratio of  $|J|$  obtained at negative ( $J_{\text{neg}}$ ) and positive ( $J_{\text{pos}}$ ) bias as a function of the absolute bias  $|V|$ . (b) Schematic representations of the junction under negative, zero, and positive biases, as described in Figure 4. The TANI–DTC SAM is depicted as being partially doped at zero bias for reasons explained in the text. For clarity, the chloride ions are not included in the scheme. The dotted line indicates the voltage profile across the junction.

between doping/dedoping steps, and not necessarily due to an intrinsic instability of the TANI–DTC monolayer toward doping and dedoping by gases.

Besides conductivity changes upon protonic doping, an intrinsic rectification effect is observed in the  $J$ – $V$  data, as shown in Figure 2b. The asymmetry is evidenced in a linear plot of the averaged data, shown in Figure 4a (as-prepared) and Figure 5a (HCl-doped). To analyze this behavior, we plotted the ratio of  $|J|$  at negative ( $J_{\text{neg}}$ ) and positive ( $J_{\text{pos}}$ ) bias as a function of  $|V|$  (insets of Figure 4a and 5a). The as-prepared sample shows little or no rectification up to around  $\pm 0.3$  V and a rectification ratio ( $\text{RR} = |J_{\text{neg}}/J_{\text{pos}}|$ ) of  $36.9 \pm 0.1$  at  $|V| = 1$  V, while the HCl-doped sample shows a more gradual increase from 0 V up to a value of  $\text{RR} = 6.2 \pm 0.2$  at  $|V| = 1$  V. We observed analogous behavior in  $14 \pm 5$  nm thick TANI layers, indicating that this effect is independent of the particular film structure (Supporting Information, Figure S12). To explain these results, we propose a model based on the enhancement of the rate constant for dissociation of water by an external electric field. This model relies on a phenomenon generally known as the second Wien (or dissociation field) effect.<sup>27,37</sup>

Figure 4b (center panel) schematically depicts a junction with the as-prepared (undoped) TANI–DTC

monolayer when  $V = 0$ , where water molecules are dynamically distributed between the TANI–DTC layer and the tail region of the hexadecanethiol layer. By analogy to phospholipid bilayer membranes, we presume that the latter comprises a region where disorder of the alkyl chains creates free volume pockets large enough to accommodate water molecules.<sup>38</sup> The left and right panels depict the situations for  $V < 0$  and  $V > 0$ , respectively. The voltage drop is expected to occur predominantly within the hexadecanethiol layer ( $d \approx 2.1$  nm), as indicated by the dotted lines, so that  $\text{H}_2\text{O}$  molecules within the tail region are exposed to the highest electric field  $E$ , and therefore the most likely to dissociate into  $\text{H}^+$  and  $\text{OH}^-$  ions. When the bias applied to the Au electrode is negative ( $V_{\text{neg}}$ ), the protons are electrostatically driven into the TANI–DTC layer, resulting in partial doping of the layer and, consequently, in an increase in its polaronic conductivity. The opposite bias ( $V_{\text{pos}}$ ) has little effect, as protons and hydroxide ions are not expected to have significant impact on the conductivity of the hexadecanethiol and TANI–DTC layers, respectively. Analogous diagrams for the HCl-doped sample are shown in Figure 5b, where the monolayer is depicted as being partially doped (i.e.,  $<2 \text{ H}^+$  per TANI–DTC molecule) when  $V = 0$  (due to loss of HCl before electrical

characterization, *vide supra*), and where hydroxide ions that are driven into the TANI–DTC layer under positive bias are presumed to react with protons to form water molecules (right panel). The dynamic doping model also accounts for the hysteresis found in the  $J$ – $V$  curves (Supporting Information, section SI-8).

To assess the feasibility of this model more quantitatively, we analyzed it according to Onsager's theory.<sup>27</sup> Onsager showed that the increase of the dissociation constant ( $k_d$ ) of a weak electrolyte due to an external electric field ( $E$ ) can be computed kinetically from the equations for Brownian motion in the combined Coulomb and external fields.<sup>27</sup> The value of  $k_d$  in a field relative to its value in the absence of a field,  $k_d(E)/k_d(0)$ , can be expressed as a function of a unitless parameter ( $b$ ) that is proportional to  $|E|$  and inversely proportional to the dielectric constant of the medium ( $\epsilon$ ). For weak electrolytes dissociating into two univalent ions, as in the case of  $\text{H}_2\text{O} \leftrightarrow \text{H}^+ + \text{OH}^-$ , the simplified expression for  $b$  is

$$b = 9.636 \times |E| / (\epsilon \times T^2) \quad (1)$$

where the units of  $|E|$  and  $T$  are  $\text{V cm}^{-1}$  and  $\text{K}$ , respectively. On the basis of previous measurements,  $\epsilon$  in the junction should be in the range 2–3.<sup>39,40</sup> With  $\epsilon = 2.5$  and  $T = 298 \text{ K}$ ,  $b = 434 \times |V|/d$ , where  $V$  is the voltage (V) applied across the junction and  $d$  (nm) is the distance over which the voltage drop occurs. With  $d = 2.1 \text{ nm}$  (*vide supra*),  $b = 207 \times |V|$ . For relatively high values of  $b$ , as in the present case, the following approximation obtained from the asymptotic expansion applies:

$$\frac{k_d(E)}{k_d(0)} = \left( \frac{2}{\pi} \right)^{1/2} (8b)^{-3/4} \exp((8b)^{1/2}) \left[ 1 - \frac{3}{8(8b)^{1/2}} \right. \\ \left. - \frac{15}{128.8b} - \frac{105}{1024((8b)^{1/2})^3} \right] \quad (2)$$

Onsager further showed that

$$\frac{\alpha(E)}{\alpha(0)} = \left\{ \frac{k_d(E)}{k_d(0)} \right\}^{1/2} \quad (3)$$

where  $\alpha(E)$  and  $\alpha(0)$  represent the degree of dissociation of water molecules in the presence and absence of the electric field, respectively.<sup>27</sup> The corresponding values of  $\alpha(E)$  can be approximated by assuming that  $\alpha(0)$  in the junction has the same value as in bulk water, that is,  $\alpha(0) = ([\text{H}^+] + [\text{OH}^-])/[\text{H}_2\text{O}] = 2 \times 10^{-7}/55.5 = 3.6 \times 10^{-9}$ . These relationships allow an estimation of the proportion of  $\text{H}_2\text{O}$  molecules that dissociate into  $\text{H}^+$  and  $\text{OH}^-$  ions in the high-field region of the junction for any applied bias  $|V|$ . This proportion,  $\alpha(E)$ , strongly depends on  $|V|$ , varying from  $3 \times 10^{-7}$  at 0.1 V to 0.13 at 1 V (Figure 6a). A combination of  $\alpha(E) = 0.13$  and a water content of  $\sim 1 \text{ H}_2\text{O}$  per TANI–DTC molecule could yield a quantity of protons sufficient to dope an as-prepared TANI–DTC monolayer to a doping percentage (DP) of  $\sim 7\%$ , where 50% corresponds to the fully doped (ES)

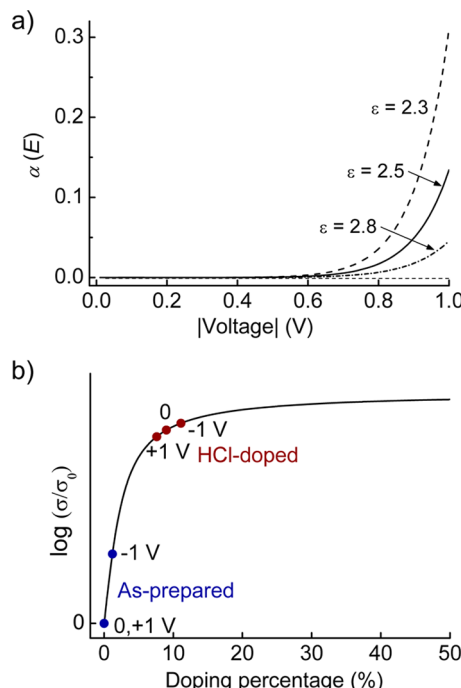


**Figure 6.** (a) Degree of dissociation  $\alpha$  versus applied voltage for water molecules exposed to an electric field  $E$  in the junctions depicted in Figures 4b and 5b. The function is computed using Onsager's equation with the parameters  $d = 2.1 \text{ nm}$ ,  $T = 298 \text{ K}$ , and  $\alpha(0) = 3.6 \times 10^{-9}$ , for three values of  $\epsilon$  (2.3, 2.5, and 2.8). (b) Asymptotic dependence of the log of relative conductivity ( $\log(\sigma/\sigma_0)$ ) on doping percentage (DP) for TANI–DTC monolayers, based on the behavior observed for PANI [ref 41]. Equal variations in the applied voltage have a stronger effect on conductivity for as-prepared TANI–DTC (steep part of the curve near  $\text{DP} = 0$ ) than for HCl-doped TANI–DTC (shallow part of the curve). Details of the derivation of this graph are provided in the Supporting Information (section SI-4).

state.<sup>41</sup> Even higher DPs would be expected if the dielectric constant  $\epsilon$  is less than 2.5; a value  $\epsilon$  of 2.3, for example, leads to  $\alpha = 0.31$  at  $|V| = 1 \text{ V}$  (Figure 6a). We note that 1  $\text{H}_2\text{O}$  per TANI–DTC molecule is a lower limit concentration to expect based on literature<sup>18,42,43</sup> and on our own XPS data (see Supporting Information, Figure S3); in fact, PANI-EB is quite hygroscopic, adsorbing up to 1  $\text{H}_2\text{O}$  per aniline unit, that is, four water molecules per TANI moiety.<sup>44–48</sup> Since TANI–DTC monolayers are exposed to ambient conditions before electrical characterization, they are likely to be hydrated and to have significantly higher water content than that detected by XPS under ultrahigh vacuum conditions. Indeed, ellipsometric measurements (under ambient conditions) yield a value  $\epsilon = 2.8$  for the static dielectric constant of the TANI–DTC SAM, which is consistent with estimations based on hydrated PANI films (Supporting Information, section SI-5).

The logarithm of electrical conductivity ( $\sigma$ ) of PANI increases asymptotically with increasing DP, as reported by Chiang and MacDiarmid,<sup>41</sup> and it is reasonable to assume that the TANI–DTC layer behaves similarly. In Figure 6b, a plot of the relative conductivity  $\sigma/\sigma_0$  versus DP is shown ( $\sigma_0$  represents the conductivity of the

as-prepared SAM). Points representing  $\sigma/\sigma_0$  under different bias conditions for as-prepared (undoped) samples are indicated on the steep part of the curve near  $DP = 0$ , while points for HCl-doped samples are drawn on the flat part of the curve. In this sense, the weaker dependence of conductivity on DP for the HCl-treated sample accounts for the smaller RR observed at  $|V| = 1$  V when compared to the as-prepared sample (i.e.,  $\sim 6$  versus  $\sim 37$ ).

Note that control experiments were carried out to verify the model based on the impact of “dry” and “wet” TANI–DTC monolayers on dynamic doping. These experiments are summarized in the Supporting Information (section SI-5). It is known that PANI (EB and ES forms) has an extremely high affinity for water<sup>44,46,49,50</sup> and that complete dehydration (at  $>200$  °C) is accompanied by decomposition of the polymer.<sup>49</sup> Such high temperatures also result in the decomposition of dithiocarbamate monolayers.<sup>30</sup> The annealing temperature used in our control experiments (70 °C) is probably insufficient to provide anhydrous TANI–DTC monolayers. Although we could observe differences in the  $J$ – $V$  characteristics of the “dry” and “wet” samples, a complete hydration/dehydration was not possible under lab conditions and therefore little additional support for the dynamic doping model could be provided. Thus, the main evidence for the dynamic doping model is given by (i) a pronounced asymmetry (and doping dependence) of the  $J$ – $V$  curves of TANI–DTC SAMs, contrasting with most monolayer-based reference junctions (showing highly symmetric  $J$ – $V$ s), (ii) the fact that neat (spin-casted) TANI films feature

qualitatively analogous  $J$ – $V$  curves as TANI–DTC SAMs, despite being structurally completely different (Figure S12), and (iii) the consistency of the hysteresis behavior with the thermodynamic trapping of  $H^+$  and  $OH^-$  ions (Figures 4a, 5a, and S6).

The second Wien (or dissociation field) effect is the basis for water-splitting in devices containing bipolar membranes,<sup>51,52</sup> and has been used to describe the nonlinear current–voltage behavior of lipid bilayer membranes.<sup>53</sup> Considering the ubiquitous nature of water, the question arises as to why the Wien effect has not been previously implicated as an influential factor in electrical measurements of thin film junctions. The answer may lie in the high proton sensitivity of the TANI–DTC monolayer, which essentially acts as a transducer, allowing an efficient conversion of the  $E$ -field generated  $H^+$  and  $OH^-$  ions into an electrical signal *via* doping or dedoping, depending on the bias polarity.

## CONCLUSION

In summary, we have demonstrated an unprecedented doping effect on the electrical conductivity of ultrathin oligoaniline monolayers, which opens up a wide range of applications from molecular electronics to chemical sensing. Furthermore, a dynamic doping–dedoping model based on field-enhanced water dissociation (Wien effect) was introduced to explain a pronounced asymmetry of the current–voltage behavior. The latter finding represents a new mechanism for modulating electrical conductivity within molecular junctions.

## METHODS

**Synthesis of Tetraaniline.** The emeraldine base of tetraaniline (TANI) was synthesized by oxidation of *N*-phenyl-1,4-phenylenediamine with ferric chloride in 0.1 M HCl followed by neutralization with ammonium hydroxide according to a published procedure.<sup>42</sup> Anal. Calcd for  $C_{24}H_{20}N_4$ : C, 79.10; H, 5.53; N, 15.37. Found: C, 77.30, 77.60; H, 5.31, 5.51; N, 14.6, 14.3.

**Sample Preparation.** (A). *Substrates.* Template-striped gold (TSG) substrates with a RMS roughness of 0.3 nm were prepared using known procedures.<sup>28</sup>

(B). *SAM Formation.* Solutions of TANI–DTC ( $\sim 5 \times 10^{-4}$  M) in ethanol were freshly prepared by an *in situ* method.<sup>29</sup> To a solution of TANI ( $5.0 \times 10^{-4}$  M, 1.80 mL) was added a solution of triethylamine (0.050 M, 18.5  $\mu$ L) and a solution of carbon disulfide (0.050 M, 18.5  $\mu$ L) to generate TANI–DTC (triethylamine salt). The solvent in each case was ethanol. Monolayers were formed by immersion, for at least 44 h, of freshly cleaved template-striped gold substrates into the solution. The samples were thoroughly rinsed with ethanol and dried in a stream of nitrogen; subsequently, they were either used immediately for measurements or stored under argon atmosphere until use.

(C). *Doping with HCl.* As-prepared samples were doped with HCl vapor by placing the samples into covered 35  $\times$  10 mm Petri dishes together with 37% HCl solution ( $\sim 20$   $\mu$ L) for 1–10 min.

**X-ray Photoemission Spectroscopy (XPS).** High-resolution XPS spectra were recorded with a Kratos Axis Ultra instrument using a monochromatized Al  $K\alpha$  (1486.6 eV) source operated at 15 kV and 180 W, with a pass-energy of 40 eV for the analyzer. Survey spectra and high resolution spectra of the S 2p, C 1s, N 1s, O 1s and Au 4f regions were acquired. The binding energies were calibrated

against the Au 4f<sub>7/2</sub> core-level peak at 84 eV. The spectra were fitted using Voigt functions with a 50/50 Lorentz/Gaussian ratio and a linear background, where the line shape parameters were adjusted by least-squares fitting to carbon and sulfur core-level signals of known alkanethiol reference samples. The S 2p spectrum, consisting of the two components S 2p<sub>3/2</sub> and S 2p<sub>1/2</sub> with a fixed separation of 1.18 eV, was fitted with a relative ratio of 2/1 for the S 2p<sub>3/2</sub>/S 2p<sub>1/2</sub> areas. The line width (fwhm) was restricted to be the same for all components in a particular spectrum.

**Electrical Measurements.** A home-built Hg-drop setup with a Hamilton syringe as Hg-dispenser was employed. The experimental setup is described in detail elsewhere.<sup>30</sup> The measurements were carried out under ambient conditions. The standard measurement protocol was as follows. The TANI–DTC SAMs on Au and a freshly extruded Hg-drop were immersed in hexadecane containing 0.001 M hexadecanethiol for 10 min, to allow the formation of a dense alkanethiol SAM on the Hg surface. Within  $\sim 1$  min after the SAM was formed, the coated drop was brought into contact with the TANI–DTC monolayer using a piezo-table, and the first  $I$ – $V$  scan was acquired. Data acquisition was performed using a voltage ramp with a bias interval of 10 mV and an elapsed time of 0.1 s between steps. The voltage ramp was carried out in the sequence  $0\text{ V} \rightarrow +1\text{ V} \rightarrow 0\text{ V} \rightarrow -1\text{ V} \rightarrow 0\text{ V}$ , with the Hg-drop being grounded. Typically, a series of 3–6 scans was obtained at the first contact location. Measurements at a second location on the same sample involved extrusion of another Hg-drop and a 10-min allowance for SAM formation on the new drop. In this way,  $I$ – $V$  characteristics at up to four locations on a single substrate could be measured, depending on the stability of the sample. The contact diameter ( $\sim 200$   $\mu$ m) between

the Hg-drop and TANI–DTC SAM was measured after each scan using a CCD-camera (side view). Current densities ( $J$ ) were thus obtained by dividing the measured current by the contact area. To exclude time-dependent dedoping and kinetic trapping, curves were only selected from the first scans in a series and shown either as individual  $J$ – $V$  curves (Figure 2b) or as geometrically averaged data (in Figures 4a and 5a, and Supporting Information, Figure S6). The error bars represent the standard error. With a typical contact area of  $\sim 3 \times 10^{-4} \text{ cm}^2$ , the  $J$ – $V$  curves represent an ensemble of  $\sim 10^{11}$  molecules.

**Conflict of Interest:** The authors declare no competing financial interest.

**Supporting Information Available:** Additional spectra and analyses, averaged  $\log(J)$ – $V$  characteristics, conductance switching by sequential acid–base treatments, details regarding  $\log(\sigma/\sigma_0)$  versus DP, control experiments with “dry” and “wet” SAMs, dependence of  $J$ – $V$  characteristics on number of scans,  $J$ – $V$  curves from reference samples, and additional evidence for dynamic doping via the Wien effect. This material is available free of charge via the Internet at <http://pubs.acs.org>.

**Acknowledgment.** We gratefully acknowledge helpful comments from Drs. Zakir Hussain, Pinar Kilickiran, Nikolaus Knorr, and Silvia Rosselli. We also thank Dr. Anthony Roberts for his support in ellipsometric measurements.

## REFERENCES AND NOTES

- Wang, D. W.; Li, F.; Zhao, J.; Ren, W.; Chen, Z. G.; Tan, J.; Wu, Z. S.; Gentle, I.; Lu, G. Q.; Cheng, H. M. Fabrication of Graphene/Polyaniline Composite Paper via *in Situ* Anodic Electropolymerization for High-Performance Flexible Electrode. *ACS Nano* **2009**, *3*, 1745–1752.
- Oyama, N.; Tatsuma, T.; Sato, T.; Sotomura, T. Dimercaptan–Polyaniline Composite Electrodes for Lithium Batteries with High Energy Density. *Nature* **1995**, *373*, 598–600.
- Inganäs, O. Hybrid Electronics and Electrochemistry with Conjugated Polymers. *Chem. Soc. Rev.* **2010**, *39*, 2633–2642.
- Wang, C.; Dong, H.; Hu, W.; Liu, Y.; Zhu, D. Semiconducting- $\pi$ -Conjugated Systems in Field-Effect Transistors: A Material Odyssey of Organic Electronics. *Chem. Rev.* **2011**, *112*, 2208–2267.
- Park, S.; Lee, T. J.; Kim, D. M.; Kim, J. C.; Kim, K.; Kwon, W.; Ko, Y. G.; Choi, H.; Chang, T.; Ree, M. Electrical Memory Characteristics of a Nondoped- $\pi$ -Conjugated Polymer Bearing Carbazole Moieties. *J. Phys. Chem. B* **2010**, *114*, 10294–10301.
- Heremans, P.; Gelinck, G. H.; Müller, R.; Baeg, K. J.; Kim, D. Y.; Noh, Y. Y. Polymer and Organic Nonvolatile Memory Devices. *Chem. Mater.* **2011**, *23*, 341–358.
- Hatchett, D. W.; Josowicz, M. Composites of Intrinsically Conducting Polymers as Sensing Nanomaterials. *Chem. Rev.* **2008**, *108*, 746–769.
- Lin, P.; Yan, F. Organic Thin-Film Transistors for Chemical and Biological Sensing. *Adv. Mater.* **2012**, *24*, 34–51.
- MacDiarmid, A. G. “Synthetic Metals”: A Novel Role for Organic Polymers (Nobel Lecture). *Angew. Chem. Int. Ed.* **2001**, *40*, 2581–2590.
- Paul, E. W.; Ricco, A. J.; Wrighton, M. S. Resistance of Polyaniline Films as a Function of Electrochemical Potential and the Fabrication of Polyaniline-Based Microelectronic Devices. *J. Phys. Chem.* **1985**, *89*, 1441–1447.
- Erokhin, V.; Berzina, T.; Camorani, P.; Smerieri, A.; Vavoulis, D.; Feng, J.; Fontana, M. Material Memristive Device Circuits with Synaptic Plasticity: Learning and Memory. *Bio-NanoScience* **2011**, *1*, 24–30.
- Chang, S. S.; Wu, C. G. Effects of Polymerization Media on the Nanoscale Conductivity and Current–Voltage Characteristics of Chemically Synthesized Polyaniline Films. *J. Phys. Chem. B* **2005**, *109*, 18275–18282.
- Wu, C. G.; Chiang, C. H.; Jeng, U. S. Phenol-Assisted Deaggregation of Polyaniline Chains: Simple Route to High Quality Polyaniline Film. *J. Phys. Chem. B* **2008**, *112*, 6772–6778.
- Lim, H.; Choi, J. H. A Comparative Study of the Polyaniline Thin Films Produced by the Cluster Beam Deposition and Laser Ablation Methods. *J. Chem. Phys.* **2006**, *124*, 014710.
- Adhikari, S.; Banerji, P. Enhanced Conductivity in Iodine Doped Polyaniline Thin Film Formed by Thermal Evaporation. *Thin Solid Films* **2010**, *518*, 5421–5425.
- Menegazzo, N.; Boyne, D.; Bui, H.; Beebe, T. P.; Booksh, K. S. DC Magnetron Sputtered Polyaniline–HCl Thin Films for Chemical Sensing Applications. *Anal. Chem.* **2012**, *84*, 5770–5777.
- Cao, Y.; Li, S.; Xue, Z.; Guo, D. Spectroscopic and Electrical Characterization of Some Aniline Oligomers and Polyaniline. *Synth. Met.* **1986**, *16*, 305–315.
- Lu, F. L.; Wudl, F.; Nowak, M.; Heeger, A. J. Phenyl-Capped Octaaniiline (COA): An Excellent Model for Polyaniline. *J. Am. Chem. Soc.* **1986**, *108*, 8311–8313.
- Shacklette, L. W.; Wolf, J. F.; Gould, S.; Baughman, R. H. Structure and Properties of Polyaniline as Modeled by Single-Crystal Oligomers. *J. Chem. Phys.* **1988**, *88*, 3955–3961.
- Wei, Z.; Faul, C. F. J. Aniline Oligomers—Architecture, Function and New Opportunities for Nanostructured Materials. *Macromol. Rapid Commun.* **2008**, *29*, 280–292.
- Wang, Y.; Tran, H. D.; Liao, L.; Duan, X.; Kaner, R. B. Nanoscale Morphology, Dimensional Control, and Electrical Properties of Oligoanilines. *J. Am. Chem. Soc.* **2010**, *132*, 10365–10373.
- Yang, Z.; Wang, X.; Yang, Y.; Liao, Y.; Wei, Y.; Xie, X. Synthesis of Electroactive Tetraaniline–PEO–Tetraaniline Triblock Copolymer and Its Self-Assembled Vesicle with Acidity Response. *Langmuir* **2010**, *26*, 9386–9392.
- Kim, H.; Jeong, S. M.; Park, J. W. Electrical Switching between Vesicles and Micelles via Redox-Responsive Self-Assembly of Amphiphilic Rod–Coils. *J. Am. Chem. Soc.* **2011**, *133*, 5206–5209.
- Udeh, C. U.; Fey, N.; Faul, C. F. J. Functional Block-like Structures from Electroactive Tetra(aniline) Oligomers. *J. Mater. Chem.* **2011**, *21*, 18137–18153.
- Guo, B.; Finne-Wistrand, A.; Albertsson, A. C. Electroactive Hydrophilic Polylactide Surface by Covalent Modification with Tetraaniline. *Macromolecules* **2011**, *45*, 652–659.
- Wang, Y.; Liu, J.; Tran, H. D.; Mecklenburg, M.; Guan, X. N.; Stieg, A. Z.; Regan, B. C.; Martin, D. C.; Kaner, R. B. Morphological and Dimensional Control via Hierarchical Assembly of Doped Oligoaniline Single Crystals. *J. Am. Chem. Soc.* **2012**, *134*, 9251–9262.
- Onsager, L. Deviations from Ohm's Law in Weak Electrolytes. *J. Chem. Phys.* **1934**, *2*, 599–615.
- Naumann, R.; Schiller, S. M.; Giess, F.; Grohe, B.; Hartman, K. B.; Kärcher, I.; Köper, I.; Lübben, J.; Vasilev, K.; Knoll, W. Tethered Lipid Bilayers on Ultraflat Gold Surfaces. *Langmuir* **2003**, *19*, 5435–5443.
- Zhao, Y.; Pérez-Segarra, W.; Shi, Q.; Wei, A. Dithiocarbamate Assembly on Gold. *J. Am. Chem. Soc.* **2005**, *127*, 7328–7329.
- von Wrochem, F.; Gao, D.; Scholz, F.; Nothofer, H. G.; Nelles, G.; Wessels, J. M. Efficient Electronic Coupling and Improved Stability with Dithiocarbamate-Based Molecular Junctions. *Nat. Nanotechnol.* **2010**, *5*, 618–624.
- Holmlin, R. E.; Haag, R.; Chabinyc, M. L.; Ismagilov, R. F.; Cohen, A. E.; Terfort, A.; Rampi, M. A.; Whitesides, G. M. Electron Transport through Thin Organic Films in Metal–Insulator–Metal Junctions Based on Self-Assembled Monolayers. *J. Am. Chem. Soc.* **2001**, *123*, 5075–5085.
- Janin, M.; Ghilane, J.; Randriamahazaka, H.; Lacroix, J. C. Electrochemical Fabrication of Highly Stable Redox-Active Nanojunctions. *Anal. Chem.* **2011**, *83*, 9709–9714.
- Lin, Y. F.; Chen, C. H.; Xie, W. J.; Yang, S. H.; Hsu, C. S.; Lin, M. T.; Jian, W. B. Nano Approach Investigation of the Conduction Mechanism in Polyaniline Nanofibers. *ACS Nano* **2011**, *5*, 1541–1548.
- Romanova, J.; Petrova, J.; Ivanova, A.; Tadjer, A.; Gospodinova, N. Theoretical Study on the Emeraldine Salt—Impact

of the Computational Protocol. *J. Mol. Struct. (THEOCHEM)* **2010**, *954*, 36–44.

- 35. Javadi, H. H. S.; Treat, S. P.; Ginder, J. M.; Wolf, J. F.; Epstein, A. J. Aniline Tetramers: Comparison with Aniline Octamer and Polyaniline. *J. Phys. Chem. Solids* **1990**, *51*, 107–112.
- 36. Wang, W.; Lee, T.; Reed, M. A. Mechanism of Electron Conduction in Self-Assembled Alkanethiol Monolayer Devices. *Phys. Rev. B* **2003**, *68*, 035416–1–035416–7.
- 37. Eckstrom, H. C.; Schmelzer, C. The Wien Effect: Deviations of Electrolytic Solutions from Ohm's Law Under High Field Strengths. *Chem. Rev.* **1939**, *24*, 367–414.
- 38. Marrink, S. J.; Berendsen, H. J. C. Simulation of Water Transport through a Lipid Membrane. *J. Phys. Chem.* **1994**, *98*, 4155–4168.
- 39. Baba, A.; Tian, S.; Stefani, F.; Xia, C.; Wang, Z.; Advincula, R. C.; Johannsmann, D.; Knoll, W. Electropolymerization and Doping/Dedoping Properties of Polyaniline Thin Films as Studied by Electrochemical-Surface Plasmon Spectroscopy and by the Quartz Crystal Microbalance. *J. Electroanal. Chem.* **2004**, *562*, 95–103.
- 40. Akkerman, H. B.; Naber, R. C. G.; Jongbloed, B.; van Hal, P. A.; Blom, P. W. M.; de Leeuw, D. M.; de Boer, B. Electron Tunneling through Alkanedithiol Self-Assembled Monolayers in Large-Area Molecular Junctions. *Proc. Natl. Acad. Sci.* **2007**, *104*, 11161–11166.
- 41. Chiang, J. C.; MacDiarmid, A. G. "Polyaniline": Protonic Acid Doping of the Emeraldine Form to the Metallic Regime. *Synth. Met.* **1986**, *13*, 193–205.
- 42. Dufour, B.; Rannou, P.; Travers, J. P.; Pron, A.; Zagórska, M.; Korc, G.; Kulszewicz-Bajer, I.; Quillard, S.; Lefrant, S. Spectroscopic and Spectroelectrochemical Properties of a Poly(Alkylthiophene)–Oligoaniline Hybrid Polymer. *Macromolecules* **2002**, *35*, 6112–6120.
- 43. Querner, C.; Reiss, P.; Bleuse, J.; Pron, A. Chelating Ligands for Nanocrystals' Surface Functionalization. *J. Am. Chem. Soc.* **2004**, *126*, 11574–11582.
- 44. Matveeva, E. S. Residual Water as a Factor Influencing the Electrical Properties of Polyaniline. The Role of Hydrogen Bonding of the Polymer with Solvent Molecules in the Formation of a Conductive Polymeric Network. *Synth. Met.* **1996**, *79*, 127–139.
- 45. Lesiak, B.; Jabłonski, A.; Zemek, J.; Trchová, M.; Stejskal, J. Determination of the Inelastic Mean Free Path of Electrons in Different Polyaniline Samples. *Langmuir* **1999**, *16*, 1415–1423.
- 46. Luzny, W.; Scniechowski, M.; Laska, J. Structural Properties of Emeraldine Base and the Role of Water Contents: X-ray Diffraction and Computer Modelling Study. *Synth. Met.* **2002**, *126*, 27–35.
- 47. Canales, M.; Aradilla, D.; Aleman, C. Water Absorption in Polyaniline Emeraldine Base. *J. Polym. Sci. B* **2011**, *49*, 1322–1331.
- 48. Casanovas, J.; Canales, M.; Fabregat, G.; Meneguzzi, A.; Aleman, C. Water Absorbed by Polyaniline Emeraldine Tends to Organize, Forming Nanodrops. *J. Phys. Chem. B* **2012**, *116*, 7342–7350.
- 49. Lubentsov, B. Z.; Timofeeva, O. N.; Khidekel', M. L. Conducting Polymer Interaction with Gaseous Substances II. PANI–H<sub>2</sub>O, PANI–NH<sub>3</sub>. *Synth. Met.* **1991**, *45*, 235–240.
- 50. Matveeva, E. S.; Diaz Calleja, R.; Parkhutik, V. P. Thermo-gravimetric and Calorimetric Studies of Water Absorbed in Polyaniline. *Synth. Met.* **1995**, *72*, 105–110.
- 51. Strathmann, H.; Krol, J. J.; Rapp, H. J.; Eigenberger, G. Limiting Current Density and Water Dissociation in Bipolar Membranes. *J. Membr. Sci.* **1997**, *125*, 123–142.
- 52. Cheng, L. J.; Chang, H. C. Microscale pH Regulation by Splitting Water. *Biomicrofluidics* **2011**, *5*, 046502–046508.
- 53. Neumcke, B.; Walz, D.; Läuger, P. Nonlinear Electrical Effects in Lipid Bilayer Membranes: III. The Dissociation Field Effect. *Biophys. J.* **1970**, *10*, 172–182.